Applied Physics B (2019) 125:219
https://doi.org/10.1007/s00340-019-7324-7

Applied Physics B
Lasers and Optics

Laser-induced emission of TiO_2 nanoparticles in flame spray synthesis

S. De Iuliis[1] · F. Migliorini[1] · R. Dondè[1]

Received: 31 January 2019 / Accepted: 4 October 2019 / Published online: 1 November 2019

Abstract
Oxide nanoparticles are widely studied because of their unique properties, including their crystalline phase, surface area, and porosity, which make them attractive for several applications. These properties are related to the increase in the surface/volume ratio when moving from the bulk to the nanoscale. For this reason, a diagnostic tool capable of monitoring the nanoparticle size and concentration during synthesis is particularly valuable. The laser-induced incandescence technique is widely used to provide such information. This study explored the applicability of this technique to TiO_2 nanoparticles in flame spray synthesis. The fluorescence, flame emission, and incandescence signals were investigated. Time-resolved spectral measurements were first carried out on TiO_2 nanoparticles deposited on a filter. At low laser fluences, the fluorescence signal of anatase TiO_2 nanoparticles was detected. At higher fluences, the incandescence signal appeared. A fluence threshold limit that depended on the matrix effect was observed, above which breakdown phenomena occur. Then, laser-induced incandescence spectral measurements were performed on the flame spray at different heights above the burner and different acquisition delay times. The analysis showed the applicability and challenges in using this diagnostic tool in flame spray synthesis.

1 Introduction

Flame spray pyrolysis (FSP) is considered a powerful method to produce nanoparticle oxides with different properties [1–4]. The possibility of changing the experimental conditions for the flame is very helpful in the synthesis of single and multicomponent nanoparticles with specific and tailored characteristics. The ability to change properties such as the crystallite size, crystalline phase, degree of aggregation and agglomeration, surface area, and porosity can have very interesting effects in different applications, including catalysis, gas sensors, and energy storage. In particular, the particle size is a key parameter in nanopowder characterization, because particle properties are often related to the surface-to-volume ratio. Monitoring the particle size during flame synthesis can be particularly attractive for the production of nanoparticles with a tailored size. To accomplish this, it would be very useful to develop a tool capable of determining the size of nanoparticles during their formation and growth in flame synthesis.

Laser-induced incandescence (LII) is a powerful diagnostic capable of providing information on the nanoparticle size and concentration [5–10]. After a pulsed laser rapidly heats a sample volume of nanoparticles, their spectral incandescence radiation intensity is measured as the nanoparticles thermally equilibrate with the surrounding gas [5, 6]. In the following, we use the expression incandescence temperature for the temperature of the nanoparticles under laser irradiation.

As reported in the literature, this technique has been widely applied to the analysis of combustion-generated carbonaceous nanoparticles, both in flames and at the exhaust of combustion systems, as well as in the environment [10–12]. The incandescence temperature and particle concentration can be obtained by performing two-color laser-induced incandescence measurements [7, 8]. Information on the particle size can be retrieved by modeling the temperature decay curve with heat transfer mechanisms [5].

Because of the wide potential of the technique, it is of great interest to investigate the applicability of LII to non-soot nanoparticles. Many papers can be found in the literature on the application of time-resolved LII (TiRe-LII) to different synthetic nanoparticles, including metallic [13–20], metalloid [14, 21–23], and oxide nanoparticles [24–26]. The

This article is part of the topical collection "Laser-Induced Incandescence".

✉ S. De Iuliis
silvana.deiuliis@cnr.it

[1] CNR-ICMATE, Institute of Condensed Matter Chemistry and Technologies for Energy, Via R. Cozzi 53, 20125 Milan, Italy

earliest attempts to perform TiRe-LII size measurements on synthetic nanoparticles were by Vander Wall et al. in [13]. The spectral and temporal signatures of TiRe-LII measurements on iron, molybdenum, titanium, and tungsten were obtained by varying the excitation laser energy density. Absorption measurements were also performed to determine the particle concentration. Fillippov et al. [19] studied ultrafine silver, graphite, and titanium nitride nanoparticles by applying TiRe-LII measurements. To this end, they made a rough assumption of the thermal accommodation coefficient, which is a key parameter in the conduction heat transfer mechanism.

More recently, different studies have considered various aspects of the application of TiRe-LII to synthetic nanoparticles. In particular, particle sizing was enabled by developing a heat transfer mechanism-based model [23 and the references therein, 15, 17, 20, 27–29].

Although much work has been done on several types of synthetic nanoparticles, only two papers can be found in the literature on TiO_2 nanoparticles [30, 31]. The lack of data concerning LII measurements on titania nanoparticles may be due to the occurrence of interference with the strong photoluminescence emission intensity. As an example, when using continuous-wave laser irradiation, a visible fluorescence band centered at approximately 505 nm of anatase TiO_2 and a near-infrared fluorescence band centered at approximately 835 nm of rutile TiO_2 are detected, which are ascribed to the oxygen vacancies in the anatase TiO_2 and to the intrinsic defects in the rutile TiO_2, respectively. [32]. Therefore, an investigation is required to distinguish the incandescence signal from the fluorescence signal, because their presence is strongly dependent on the experimental conditions under analysis.

In previous works [30, 31], measurements were performed in an aerosol flame reactor using the fourth harmonic (266 nm) of an Nd:YAG laser while varying the laser fluence. Time-resolved LII measurements were carried out, and the dependence of the decay time on the particle size was experimentally demonstrated. As preliminary results, a correlation between the decay time and the nanoparticle diameter measured from TEM micrographs was obtained, proving the feasibility of using the technique to monitor the TiO_2 nanoparticle size in such a reactor. However, only preliminary measurements have been performed on this particular hybrid reactor under analysis, and no quantitative correlation of the TiO_2 particle diameter with the decay rate has been obtained.

The aim of this work was to explore the applicability of laser-induced incandescence to TiO_2 nanoparticles in an FSP apparatus. FSP is a synthesis process that is suitable for the industrial scale production of oxide nanoparticles. In contrast to an aerosol flame reactor, in FSP, the combustion process is characterized by a high temperature and particle concentration, resulting in a very luminous and optically thick flame. This is particularly challenging for an optical technique like LII, which has not previously been explored.

As a first approach, time-resolved laser-induced emission measurements were performed on TiO_2 nanoparticles deposited on a filter to investigate the main features of the spectral emission by changing the laser energy density and detection delay time with respect to the laser energy peak. A range of fluences were tested for LII measurements, to explore the occurrence of different phenomena such as the fluorescence, incandescence, and breakdown. By analyzing the temporal behavior of the signals at different laser fluences, it was also possible to evaluate the lifetimes of these phenomena and the related interferences.

The optical apparatus used for the spectral LII measurements was then directly applied to the flame spray. The investigation was performed on the flame axis using various heights above the burner (HAB). The analysis showed the applicability of this diagnostic tool to flame spray synthesis.

2 Experimental

2.1 Optical setup

The experimental setup employed for the laser-induced emission measurements is shown in Fig. 1. The fourth harmonic (266 nm) of a pulsed Nd:YAG laser (Quanta System S.p.A.) was used, because this wavelength was within the UV spectral absorption band of the TiO_2 nanoparticles. Tto obtain a uniform heating temperature, a portion of the laser beam was selected with a diaphragm ($\varnothing = 8$ mm) and focused on the target (filter/flame) by means of a lens. The radiation emitted by the nanoparticles was collected by a lens ($f = 225$ mm) and focused on a 3 mm-diameter optical fiber, which was connected to the entrance slit of a spectrograph (Shamrock

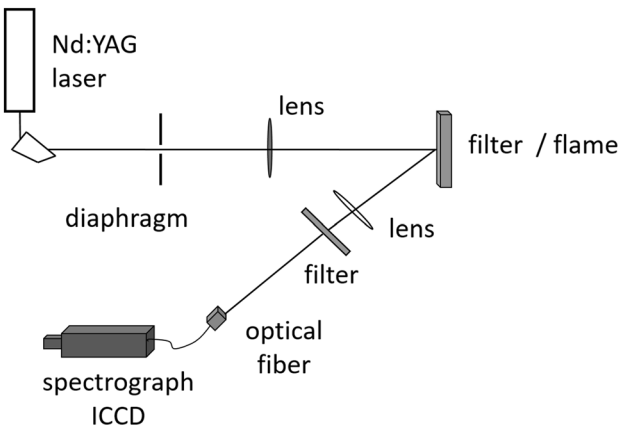

Fig. 1 Experimental setup for laser-induced emission measurements

303i) coupled with an ICCD camera (iSTAR 334T, Andor Technology). Because 1:1 magnification was used for the collection optics, a spatial resolution of 3 mm was obtained. A 305 nm high-pass filter was positioned in front of the receiving optic to remove the reflection of the 266 nm laser beam. Moreover, to reduce the 532 nm second harmonic of the laser, a notch filter was also added in front of the detector. In fact, although it deviated from the detection path as the result of a Pellin Broca prism, the green beam persisted after frequency doubling. This filter was removed when performing emission intensity measurements using long delays with respect to the laser pulse. The spectral emission was collected using a 150 grooves/mm grating (0.28 nm resolution). The features of the signal were analyzed by changing the laser fluence, as well as the delay time of the acquisition gate with respect to the laser pulse.

Measurements were performed on TiO_2 nanoparticles produced via FSP. Ex situ measurements were performed as a preliminary investigation to explore the spectral emission signature of the TiO_2 nanoparticles. To this end, nanoparticles deposited on a glass fiber filter were investigated. For relatively low laser fluences, each spectrum was the result of the accumulation of 100 acquisitions, as will be discussed later in detail. In contrast, for higher laser fluences, a significant decrease in the emission intensity with time was detected in multiple shot spectral measurements. Thus, in this case, single-shot measurements were considered.

The same optical arrangement was applied to measure the radiation intensity emitted by the nanoparticles during flame synthesis. To this purpose, the spectral emissions on the flame axis at different HABs were detected. Moreover, to check the effect of the laser irradiation and discriminate the laser-induced incandescence from the flame emission, measurements were carried out with and without the laser, by alternately collecting the laser-induced emission and flame emission. This was accomplished by doubling the trigger frequency of the spectrometer with respect to the laser frequency. The data were acquired by collecting 100 single shots. Because of the typical nanoparticle residence time in the probe volume (on the order of tens of microseconds) and the laser frequency used (5 Hz), a fresh probe volume was considered for each laser shot.

To investigate the optical properties of the TiO_2 nanoparticles produced in the flame, extinction measurements were carried out on nanoparticle deposits. A calibrated deuterium lamp (Oriel) was used as a light source, and the transmitted signal was collected on an optical fiber connected to a spectrometer (TM-CCD-A series, Hamamatsu). To obtain a uniform titania deposit, nanoparticles were collected on a glass plate using a fast insertion in the synthesis flame. The optimal insertion procedure was tested by changing the residence time of the collecting probe. The aim was to collect enough particles to detect the absorption while still allowing transmittance measurements. The value of the residence time used was on the order of 100 ms.

2.2 Flame spray pyrolysis apparatus

Figure 2 shows the FSP apparatus [33]. It was essentially an oxygen-assisted spray apparatus, where the precursor was injected coaxially with the pilot fame. For the pilot flame, a lamella burner was used to produce a sustained methane/air lean premixed flame with an equivalence ratio of 0.8. The spray was obtained using a custom-made stainless steel gas-assisted spray injector consisting of a capillary inserted in the gas nozzle. The precursor solution flowed through the capillary in a stream of oxygen used as a nebulizing gas. The resulting droplets started to react with the oxygen in a diffusion flame. By changing the fuel and oxygen flow rates, the experimental conditions of the flame were changed (i.e., the temperature field, gas velocity, residence time, and fuel/oxygen ratio).

Titanium tetraisopropoxide (Sigma-Aldrich, 97% purity) dissolved in ethanol (0.5 M) was used as a liquid precursor. The solution was injected at a feed rate of 4 ml/min through the spray nozzle by means of a syringe pump and nebulized using an O_2 stream with a flow rate of 5 Nl/min. A synthesis flame with a height of approximately 8 cm was obtained. TiO_2 nanoparticles were produced and collected on a glass fiber filter (150 mm diameter, Whatman Grade *G*F/A Glass Microfiber filter) downstream of the reactor using a vacuum pump system for ex situ measurements. Under these conditions, the primary nanoparticle diameter was less than 20 nm, as measured in an STEM analysis.

3 Results and discussion

3.1 Nanoparticle absorption measurements

To derive the absorption coefficient, extinction measurements were performed on the TiO_2 nanoparticles deposited on the glass plate. According to the Lambert–Beer law, the monochromatic transmissivity, that is the ratio of the transmitted ($I_{\lambda T}$) to incident light ($I_{\lambda 0}$), can be expressed as follows [34, 35]:

$$\tau_\lambda = \frac{I_{\lambda T}}{I_{\lambda 0}} = \exp\left(-\int_0^L K_{\mathrm{ext},\lambda}\,\mathrm{d}x\right), \tag{1}$$

where $K_{\mathrm{ext},\lambda}$ is the extinction coefficient of the nanoparticles, x is the spatial location along the path crossed by the laser beam, and L is the length of the chord through the medium.

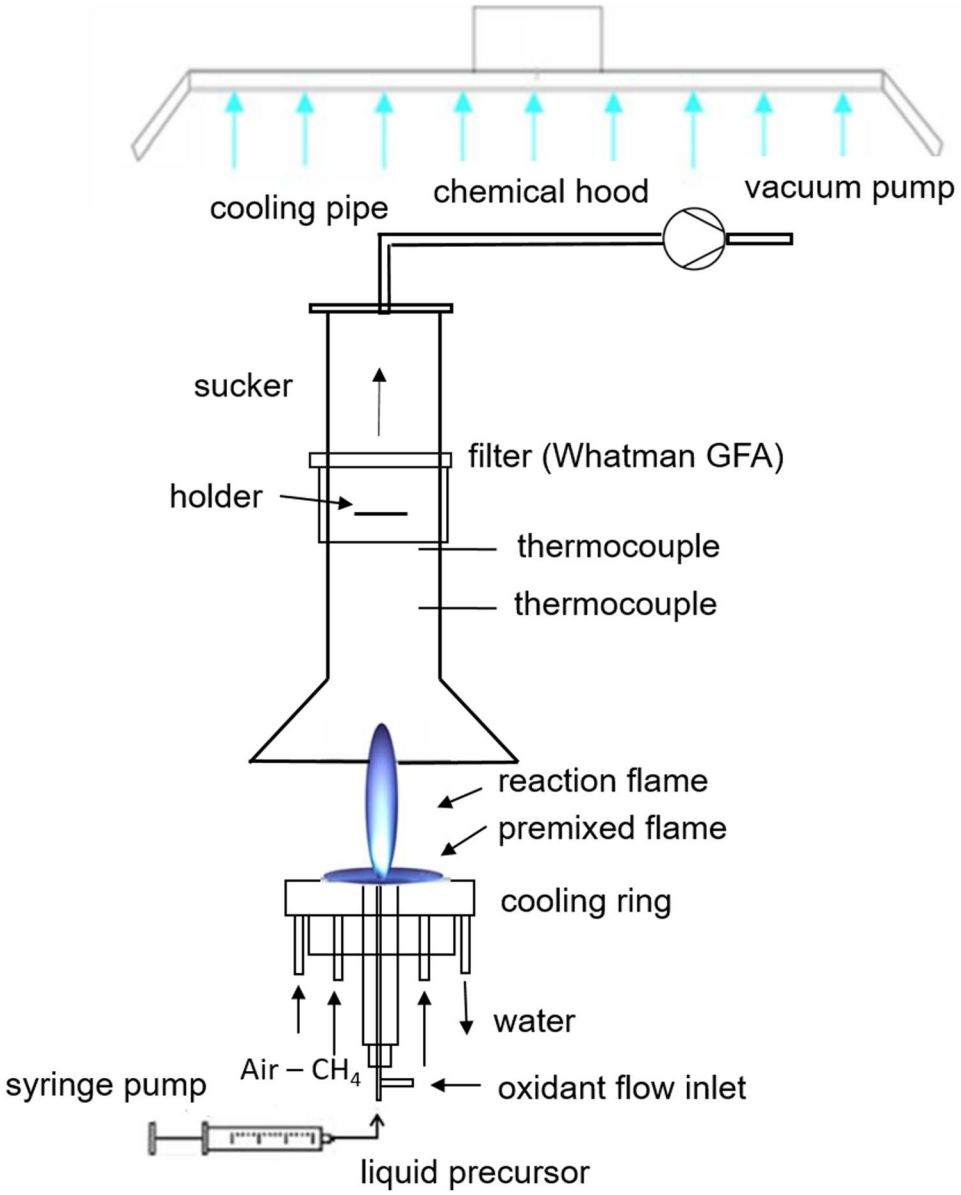

Fig. 2 Flame spray pyrolysis apparatus

If the particles are homogenously distributed in the medium, Eq. 1 can be simplified as follows:

$$-\ln \tau_\lambda = \frac{I_{\lambda T}}{I_{\lambda 0}} = K_{\text{ext},\lambda} L. \tag{2}$$

The extinction coefficient can be expressed as follows:

$$K_{\text{ext},\lambda} = K_{\text{abs},\lambda} + K_{\text{scatt},\lambda}, \tag{3}$$

where $K_{\text{abs},\lambda}$ and $K_{\text{scatt},\lambda}$ are the wavelength-dependent absorption and scattering coefficients, respectively. If the scattering contribution is considered negligible, the transmittance measurements allow for the direct measurement of the absorption coefficient. This hypothesis is justified by the relatively small size of the particle under study (less than 20 nm). Moreover, assuming Kirchhoff's law to be valid, the particles absorbing and emitting thermal radiation are at thermodynamic equilibrium, and the spectral emissivity, $\epsilon(\lambda)$, of the nanoparticles sampled on the glass plate can be derived from absorption measurements as follows:

$$\epsilon(\lambda) = 1 - \exp\left(-K_{\text{abs},\lambda} L\right). \tag{4}$$

Figure 3 shows the spectral behavior of the emissivity in the 300–600 nm spectral range. The emissivity exhibits a fast decrease up to 400 nm and a slower one toward higher wavelengths. This curve was used for signal processing, as described in the next section. The same emissivity curve was used at every measurement location in the flame, assuming that no changes in the particle optical properties occurred along the flame. To consider these possible changes, in situ measurements would be more appropriate. However, an

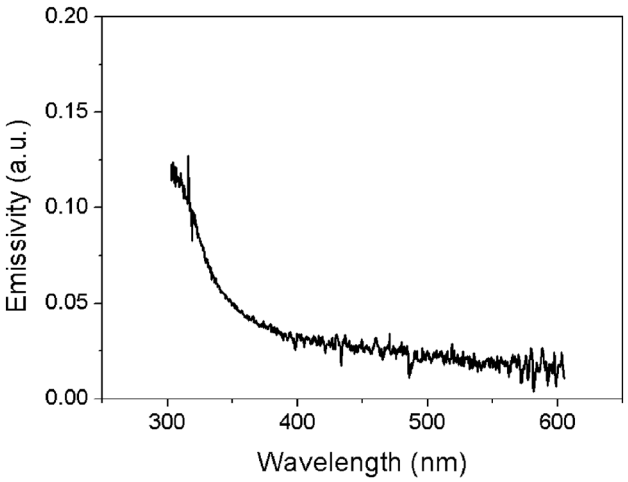

Fig. 3 TiO_2 emissivity versus wavelength

optical in situ analysis would be quite challenging in our luminous flame, and thus will be object of a future study.

3.2 Laser-induced emission measurements on filter

To investigate the spectral behavior of the laser-induced emission intensity when changing the laser fluence, measurements were performed on nanoparticles deposited on the glass fiber filter. The spectral emission was collected at different acquisition delay times. As an example, Fig. 4 shows the spectra obtained at 0.7 mJ/cm^2. Each spectrum is the result of the accumulation of 100 measurements collected with a detection gate width of 100 ns. Two different and well-defined emission bands can be observed at a short delay time (100 ns): one in the UV spectral region centered at approximately 360 nm and the other in the green spectral region centered at approximately 480–490 nm. When the delay time was increased, while the emission band in the green spectral region decreased, the 360 nm emission band persisted up to a 500 ns delay. The two bands corresponded to known fluorescence features and were characterized by different signal decay times. The fluorescence signal detected at approximately 480 nm was related to defect states in the anatase TiO_2 nanoparticles, and particularly to the oxygen vacancies located on the (101) surface, in agreement with the results reported in the literature [32]. The green band consisted of sub-bands related to the above-mentioned defects in the particle structure. Therefore, the balance between these contributions could result in a shift in the fluorescence peak [36]. The emission band in the UV spectral region was attributed to the fluorescence signal intensity of the glass fiber filter used to collect TiO_2 nanoparticles, as shown in Fig. 5, where the fluorescence spectrum from the clean filter is reported. Moreover, the same figure shows the overall fluorescence spectra collected at different laser fluencies, which were measured by accumulating 100 spectra using a 100 ns delay time. The spectra were normalized to the maximum intensity value of the filter fluorescence spectrum. The peak at 532 nm can be attributed to the second harmonic of the laser beam, which persisted after frequency doubling. As can be seen, increasing the laser fluence resulted in a decrease in the green spectral band intensity. This behavior was related to the effect of laser irradiation on the

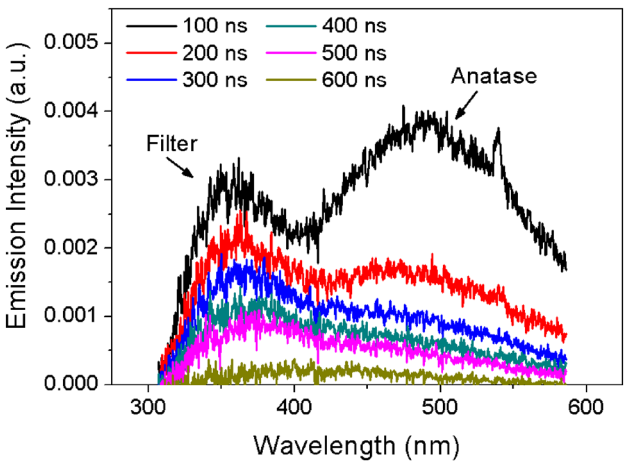

Fig. 4 Laser-induced emission spectra of TiO_2 nanoparticles deposited on glass fiber filter at different delay times and at 0.7 mJ/cm^2 laser fluence. In the graph, the UV band is due to the filter fluorescence, and the green band is the result of the anatase nanoparticle fluorescence. Spectra were collected by accumulating 100 measurements

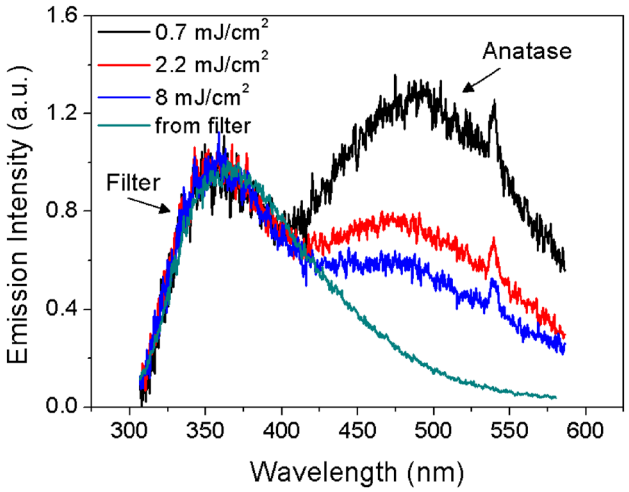

Fig. 5 Fluorescence spectra of TiO_2 nanoparticles deposited on glass fiber filter collected at different laser fluences and at 100 ns delay time. In the figure, the fluorescence from the filter is also reported. All of the curves were normalized to the intensity value at 370 nm. Spectra were collected by accumulating 100 measurements

filter-deposited nanoparticles, which resulted in an artifact. In fact, for laser fluences lower than 1 mJ/cm^2, no significant change in the emission spectrum was observed during the accumulation process. For laser fluences of up to 8 mJ/cm^2, a progressive decrease in the TiO_2 fluorescence during accumulation was observed. This was interpreted to be the result of the gradual ablation of the TiO_2 nanoparticles from the filter. Single-shot measurements could be more effective in the evaluation of the fluorescence signal, but in this case, very poor signal-to-noise ratio would be obtained because of the low laser fluence and low concentration of nanoparticles on the filter.

For higher laser fluences, the occurrence of shock waves was clearly revealed by acoustic noise. Moreover, a strong decrease in the emission signal was already detected after the first laser shot, confirming the ablation of the nanoparticles. Thus, in this case, the measurements were performed by collecting the signal from a single laser shot at a given filter position. Consecutive signals were collected by moving the filter to probe a fresh spot (i.e., one not affected by the previous laser shots). Thirty single-shot measurements were carried out for each condition.

Figure 6a shows the spectral emission intensity collected at a laser fluence of 17 mJ/cm^2 in the single-shot mode at delay times ranging from 100 ns to 1000 ns. As can be seen, a completely different behavior of the laser-induced emission is observed compared to the fluorescence spectra reported in Figs. 4 and 5. For each signal, a typical continuous broad-band LII spectrum is observed, which tends to increase moving toward the IR spectral region, in agreement with the data reported in [30, 31].

Because incandescence is a type of thermal emission, the radiation intensity I_p emitted at a given wavelength λ by a concentration of particles heated at a temperature T_p is given by the following relationship:

$$I_P(T_P,c) = \tau_\lambda R_{BB}(T_P,\lambda)\epsilon(\lambda), \tag{5}$$

where R_{BB} is the blackbody energy spectral density, as given by Planck's law; T_p is the temperature of the heated particles; ϵ is the wavelength-dependent monochromatic emissivity of the cloud of nanoparticles; and τ_λ is an instrument function that takes into account geometric and spectral factors of the detection system. The above relationship is the basis of the pyrometry usually applied in luminous flames. The instrument function was obtained by placing a calibrated tungsten ribbon lamp at the same location as the flame or nanoparticle-deposited filter. Then, the spectral emission was collected under the same experimental conditions as the emission/incandescence measurements.

Considering the experimental curve, which was corrected for both the instrument function and TiO_2 nanoparticle emissivity, an evaluation of the incandescence temperature could be made using Eq. (5). To this end, the spectral emissivity derived from the absorption coefficient, as shown in Fig. 3, was used. By applying this procedure to the raw data reported in Fig. 6a, the corrected spectra and related fitting curve were obtained and are shown in Fig. 6b. The resulting values for the incandescence temperature are also reported in the legend, and their behavior versus delay time is shown in Fig. 7.

By fitting each spectrum of a set of thirty, an average relative error of 1.6% was found for the temperature. The observed variations between laser shots were random and related to a Gaussian distribution. Therefore, the noise could be modeled as done in [37]. The maximum value of incandescence temperature detected was 3020 K, which

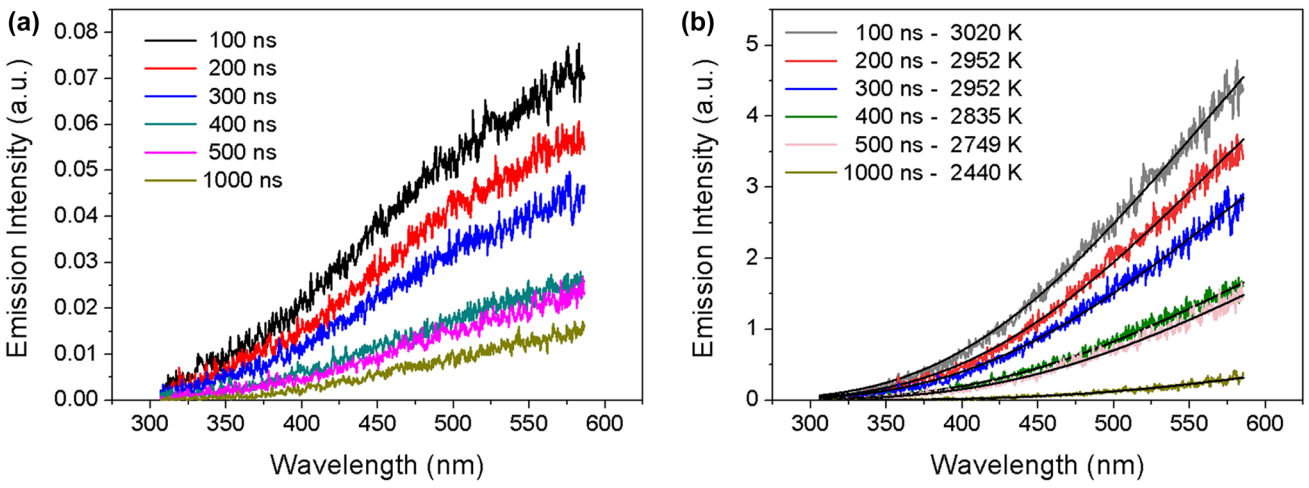

Fig. 6 Laser-induced incandescence of TiO_2 nanoparticles deposited on glass fiber filter at 17 mJ/cm^2 laser fluence. In (**a**), raw spectra are reported, whereas in (**b**), the spectra are corrected for the instrument function and particle emissivity, and fitted by Planck's law. Spectra were collected using the single-shot mode

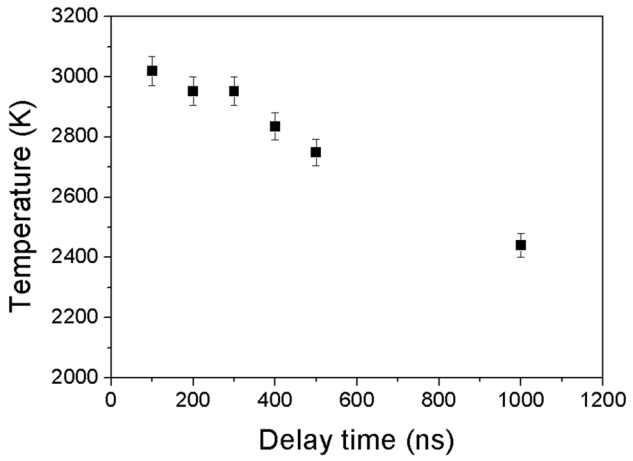

Fig. 7 Incandescence temperature of nanoparticles deposited on glass fiber filter versus delay time

was less than the sublimation temperature of the TiO_2 bulk. At a delay time of 1000 ns, the incandescence temperature decreased to approximately 2440 K, which was the lowest detectable temperature under our experimental conditions.

Figure 6 shows that the laser-induced incandescence becomes predominant at delay times longer than 100 ns. However, at shorter delay times, the fluorescence emission can still be observed in this laser fluence region. This observation demonstrated the different lifetimes of the two signals (fluorescence and incandescence) under analysis. As an example, in Fig. 8, the spectral behavior of the emission signal is reported for delay times from 10 ns up to 50 ns, with a detection gate width of 10 ns. These spectra were obtained at the same laser fluence used for the data in Fig. 6. The spectra were collected in the spectral range of 350–650 nm and using a 532 nm notch filter in front of the detector to reduce the second harmonic contribution, which was significant close to the laser pulse. Although a correction for the instrument function was performed, the second harmonic contribution is still evident in each spectrum. At a very short delay time (10 ns), the fluorescence emission spectrum in the green spectral region is shown, which is attributed to anatase TiO_2 emission, as already observed in Fig. 5. However, moving to longer delays, the fluorescence band significantly decreases, and the incandescence signal starts to appear. Because of the difference in the characteristic lifetimes of the fluorescence and incandescence, as shown in this figure, it is possible to discriminate the occurrence of these phenomena. By delaying the measurements to more than 50 ns after the laser shot, the fluorescence contribution can be neglected.

LII spectra similar to the ones shown in Fig. 6 were obtained by increasing the laser fluence up to a threshold limit, above which other phenomena occurred. In particular, Fig. 9 shows the spectral laser-induced emission obtained at 56 mJ/cm^2 and detected at a delay time of 100 ns. The presence of emission peaks on a continuous background is evident. Such peaks were the result of the occurrence of laser-induced breakdown phenomena, in agreement with [30, 31]. The laser energy density was high enough to produce a micro-plasma in the probe volume, where the molecules were dissociated and excited. The resulting emission signal was characterized by atomic lines on a continuous emission. In our measurements, breakdown phenomena already occurred at a relatively low laser fluence value of approximately 50 mJ/cm^2. This was due to the presence of the glass fiber filter, which introduced a significant matrix effect. In fact, the physical and chemical properties of the sample could significantly affect the plasma composition. As a result, the emission line intensity and fluence threshold

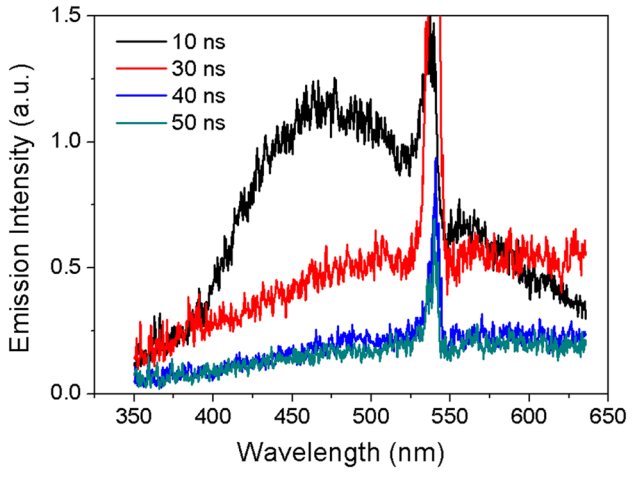

Fig. 8 Laser-induced emission of TiO_2 nanoparticles deposited on glass fiber filter at 17 mJ/cm^2 laser fluence and short delay times (10–50 ns). Spectra were collected using the single-shot mode

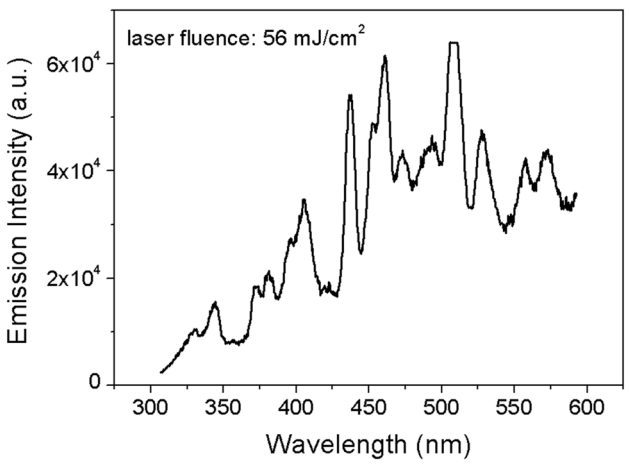

Fig. 9 Laser-induced breakdown intensity versus wavelength at 56 mJ/cm^2 laser fluence and 100 ns delay time

where plasma radiation became visible were dependent on the concentration of the element under analysis, as well as on the properties of the matrix that contained it. Therefore, care had to be taken in relation to the particular experimental conditions under analysis. The threshold limit above which laser-induced breakdown started to occur could be completely different under other conditions such as a nanoparticle aerosol.

3.3 Flame spray emission

The luminosity of the flame was mainly due to the light emitted by the nanoparticles. The emission due to the chemiluminescence was negligible compared to the thermal emission of the particles. Therefore, in the following, the flame emission and flame temperature refer to the emission and temperature of the particles present in the flame in the absence of laser heating.

To investigate the applicability of laser-induced incandescence to FSP, it was important to measure the initial temperature of the nanoparticles in the flame and the value obtained under laser irradiation. To this purpose, flame emission measurements were collected alternately with respect to the incandescence emission measurements. The data were acquired by collecting 100 spectra.

This section reports the flame emission measurements to evaluate the flame temperature. Under our conditions, a very high temperature was expected because of the use of pure oxygen as an oxidizer. As a rough estimation, the adiabatic temperature of an ethanol/oxygen flame is approximately 2900 K [38]. A whitish emission was observed from the synthesis flame, which made measurements of the laser-induced emission very challenging. In fact, laser heating would be effective in a limited temperature range, from the flame to TiO_2 sublimation temperature. Measurements were performed at HAB values of 2 cm, 4 cm, 6 cm, and 8 cm. Figure 10a shows the resulting emission signal intensities corrected for the instrument function and emissivity versus the wavelength. The same figure shows the fitting curves, and the derived temperature values are reported in the legend. The signal decreases in intensity moving upward in the flame and becomes negligible at the flame tip (HAB = 8 cm, not shown in Fig. 10a). The axial flame temperature profile versus HAB is reported in Fig. 10b. A temperature value close to 3000 K is observed low in the flame, which decreases slightly at higher HABs. Because the flame temperature was close to the values obtained from the laser-induced emission of nanoparticles deposited on the filter (Fig. 7), it was clear that the application of laser-induced incandescence on a flame spray was quite challenging, because breakdown effects would prevent the LII temperature from greatly exceeding the flame temperature.

3.4 Laser-induced incandescence in flame spray

Laser-induced incandescence measurements were made in the flame spray at a laser fluence selected to avoid both fluorescence contributions from the anatase TiO_2 nanoparticles and breakdown. For measurements in the flame, because of the different matrix effects (filter vs. flame), a threshold fluence limit of approximately 150 mJ/cm^2 was observed for the breakdown. Consequently, a relatively wide range of laser fluence values could be considered when examining the laser-induced incandescence in our flame spray. Moreover, as already observed in the previous section, the chosen value of laser fluence should allow the heating of nanoparticles above the initial flame temperature up to their sublimation condition.

The incandescence signal was collected alternately with respect to the flame emission at HAB values of 2 cm, 4 cm,

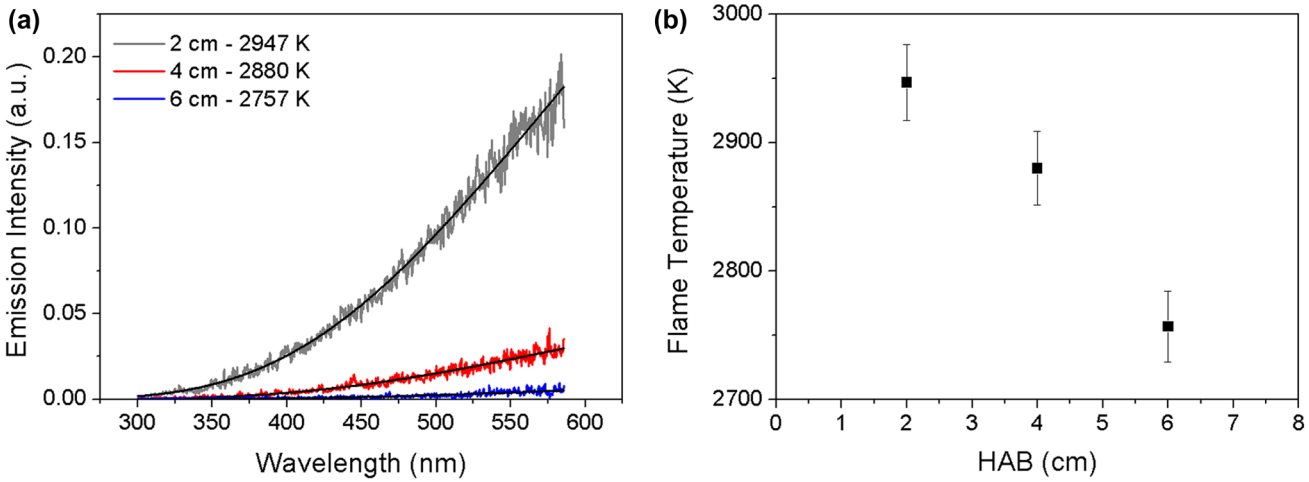

Fig. 10 Flame emission at HAB = 2 cm, 4 cm, and 6 cm: **a** spectral intensity and **b** flame temperature

6 cm, and 8 cm. The spectral emission was investigated at different detection delay times. For the LII emission, measurements were performed at a laser fluence of 80 mJ/cm^2 to avoid breakdown and at a decay time longer than 50 ns to neglect fluorescence. Spectra were corrected for the instrument function and particle emissivity and fitted by Planck's law.

As an example, Fig. 11a shows the laser-induced incandescence spectra obtained when changing the delay time from 100 ns to 800 ns. The data refer to measurements performed at HAB = 2 cm. The experimental detection gate width used was 100 ns. As shown in the figure, a decrease in the signal intensity was observed with an increase in the delay time. The spectral flame emission collected at the same flame height is also reported for comparison. The LII emission remains higher than the flame emission up to a delay of 800 ns. Figure 11b shows the corresponding LII temperature versus delay time, as well as the flame temperature. The incandescence temperature is higher than the flame temperature up to 300 ns. For longer delays, the two temperatures are consistent within the measurement uncertainties (approximately 1% relative error, obtained from 100 spectra).

In Fig. 12, LII measurements at 2 cm, 4 cm, 6 cm, and 8 cm HAB are shown. The spectral behavior refers to a laser fluence of 80 mJ/cm^2 and a delay time of 100 ns. Moving higher in the flame, a significant decrease in the signal intensity is detected. In fact, because of the spray gas entrainment, the nanoparticle concentration in the probe volume decreases with HAB. Using Eq. (5) and fitting the spectra using Planck's law, a nanoparticle temperature value of approximately 3150 K is obtained for all HABs, independently from the initial flame emission temperature values. This could indicate a similar distribution of the particle diameters or a trade-off between the effects of the diameter and surrounding gas temperature on the cooling rate of the particles.

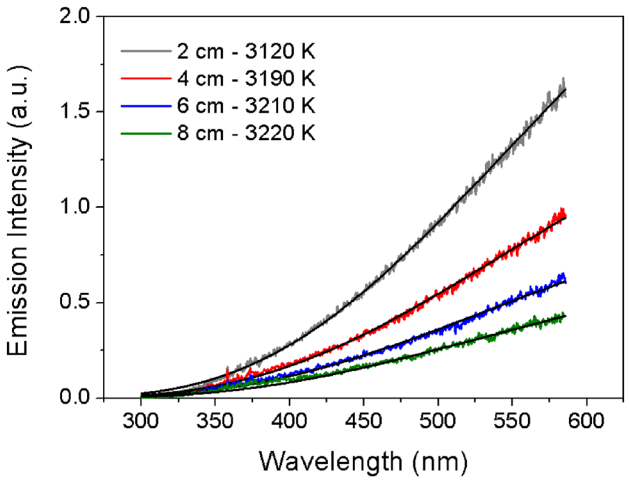

Fig. 12 Laser-induced incandescence spectra at 80 mJ/cm^2 and different HABs

4 Conclusions

TiO_2 nanoparticles deposited on both a filter and in the flame of an FSP reactor were irradiated with the fourth harmonic of a pulsed Nd:YAG laser to study the applicability of laser-induced incandescence as a monitoring tool during the synthesis process. To investigate the main spectral features of the laser-induced emission signal while changing the laser fluence, an analysis was first performed on the nanoparticles deposited on a filter. At a relatively low laser fluence

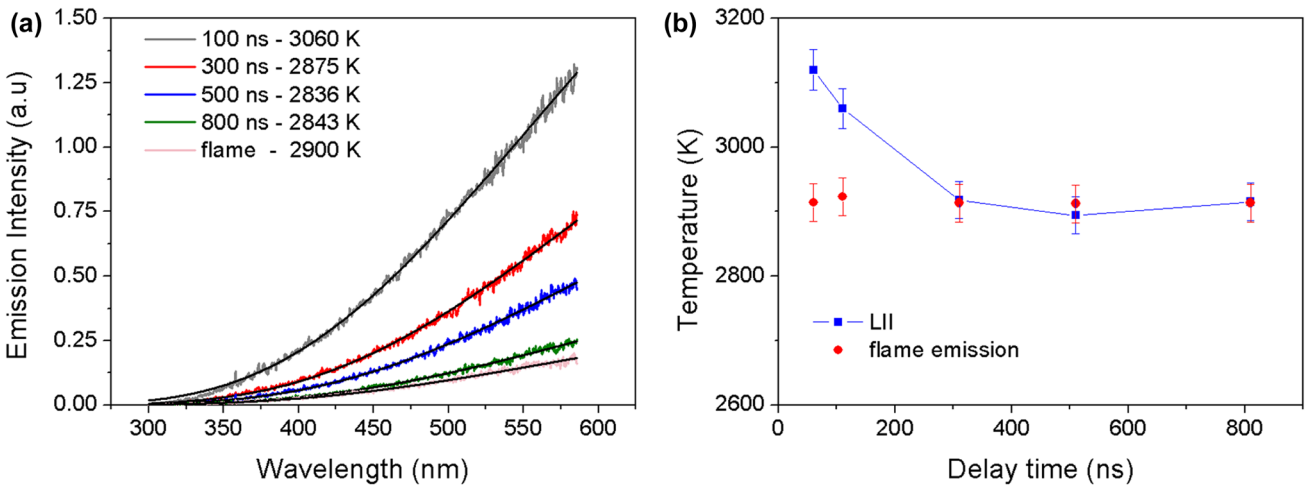

Fig. 11 Comparison of spectral LII signal with flame emission at HAB = 2 cm (**a**) and incandescence temperature vs. delay time and flame temperature (**b**)

(< 8 mJ/cm^2), a fluorescence signal was detected in the green spectral region (with a peak in the range of 480–490 nm). This was attributed to anatase TiO_2 and was due to the oxygen vacancies located on the (101) surface. Moving to a higher laser fluence, the incandescence signal overwhelmed the fluorescence signal, which, although still present below a delay time of 50 ns, could be completely neglected for longer acquisition delay times. At even higher laser fluences, breakdown phenomena occurred. The threshold value for the laser fluence was strictly related to matrix effects, and consequently depended on the particular experimental conditions under analysis.

The results obtained from the particles deposited on the filter were used as guidelines for the LII measurements in the flame spray. However, in this case, the initial temperature of the TiO_2 nanoparticles before laser heating had to be considered. In fact, the temperature of a fuel/oxygen flame could be very close to the TiO_2 sublimation temperature. If the two temperatures were almost identical, no temperature increase could be obtained by laser irradiation. Therefore, both flame and LII emission measurements were performed at different HABs. The LII emission measurements were performed at a laser fluence of 80 mJ/cm^2 to avoid breakdown and at a delay time longer than 50 ns to neglect fluorescence. Under these conditions, the LII emission was higher than the flame emission up to a delay of 800 ns. For delays equal to or longer than 100 ns, the incandescence temperature values ranged from the flame temperature (~ 2900 K) to approximately 3150 K, which was below the TiO_2 boiling point. The LII temperature remained higher than the flame temperature up to a certain delay value, depending on the HAB under analysis (300 ns for HAB = 2 cm). This temperature difference allowed a cooling transient whose modeling could give in situ information on the nanoparticle size.

These results proved the applicability of the LII technique to the TiO_2 flame spray synthesis. Future work will be devoted to in situ optical property measurements and time-resolved measurements for nanoparticle size monitoring.

Acknowledgements The authors acknowledge the fruitful technical support provided by Mr. Gianni Brunello. This work was supported by the I-ZEB project (Towards Intelligent Zero Energy Buildings for a smart city growth), in the framework of the Accordo Quadro Regione Lombardia/CNR.

References

1. L. Madler, H.K. Kammler, R. Mueller, S.E. Pratsinis, J. Aerosol. Sci. **33**, 369–389 (2002)
2. R. Strobel, A. Baiker, S.E. Pratsinis, Adv. Powder Technol. **17**(5), 457–480 (2006)
3. R. Koirala, S.E. Pratsinis, A. Baiker, Chem. Soc. Rev. **45**, 3053–3068 (2016)
4. A.J. Grohn, S.E. Pratsinis, A. Sanchez-Ferrer, R. Mezzenga, K. Wegner, Ind. Eng. Chem. Res. **53**, 10734–10742 (2014)
5. H.A. Michelsen, C. Schultz, G.J. Smallwood, S. Will, Prog. Energy Combust. Sci. **51**, 2–48 (2015)
6. C. Schultz, B.F. Kock, M. Hofmann, H. Michelsen, S. Will, B. Bourgie, R. Suntz, G. Smallwood, Appl. Phys. B **83**(3), 333–354 (2006)
7. S. De Iuliis, F. Cignoli, G. Zizak, Appl. Opt. **44**(34), 7414–7423 (2005)
8. D.R. Snelling, G.J. Smallwood, F. Liu, O.L. Gulder, W.D. Bachalo, Appl. Opt. **44**(31), 6773–6785 (2005)
9. S. De Iuliis, F. Migliorini, F. Cignoli, G. Zizak, Proc. Combust. Inst. **31**(1), 869–876 (2007)
10. F. Migliorini, S. De Iuliis, S. Maffi, G. Zizak, Appl. Phys. B **112**(2), 433–440 (2013)
11. F. Migliorini, S. De Iuliis, S. Maffi, G. Zizak, Appl. Phys. B **120**, 417–427 (2015)
12. S. De Iuliis, F. Migliorini, F. Cignoli, G. Zizak, Appl. Phys. B **83**, 397–402 (2006)
13. R.L. Vander Wall, T.M. Ticich, J.R. West, Appl. Opt. **38**(27), 5867–5879 (1999)
14. T.A. Sipkens, Advances in the Modeling of Time-Resolved Laser-Induced Incandescence PhD Thesis, University of Waterloo, Ontario, Canada, 2018
15. Y. Murakami, T. Sugatani, Y. Nosaka, J. Phys. Chem. A **108**(40), 8994–9000 (2005)
16. T.A. Sipkens, N.R. Singh, K.J. Daun, Appl. Phys. B **123**(1), 14–30 (2017)
17. A. Eremin, E. Gurentsov, C. Schulz, J. Phys. D Appl. Phys. **41**, 1–5 (2008)
18. S.T. Moghaddam, K.J. Daun, Appl. Phys. B **124**(8), 159–178 (2018)
19. A.V. Fillipov, M.W. Markus, P. Roth, J. Aerosol. Sci. **30**(1), 71–87 (1999)
20. B.F. Kock, C. Cayan, J. Knipping, H.R. Orthner, P. Roth, Proc. Combust. Inst. **30**, 1689–1697 (2005)
21. G.S. Eom, C.W. Park, Y.H. Shin, K.H. Chung, S. Park, W. Choe, J.W. Hahn, Appl. Phys. Lett. **83**(6), 1261–1263 (2003)
22. J. Menser, K. Daun, T. Dreier, C. Schulz, Appl. Phys. B **122**(11), 277 (2016)
23. T.A. Sipkens, R. Mansmann, K.J. Daun, N. Petermann, J.T. Titantah, M. Karttunen, H. Wiggers, T. Dreier, C. Schutz, Appl. Phys. B **116**, 623–636 (2014)
24. R. Mueller, L. Madler, S.E. Pratsinis, Chem. Eng. Sci. **58**, 1969–1976 (2003)
25. D. Allen, H. Krier, N. Glumac, J. Heat Transf. **138**(11), 112401 (2016)
26. P. Roth, Proc. Combust. Inst. **31**, 1773–1788 (2007)
27. K.J. Daun, Int. J. Heat Mass Transf. **52**(21), 5081–5089 (2009)
28. K.J. Daun, J.T. Titantah, M. Karttunen, Appl. Phys. B **107**(1), 221–228 (2012)
29. K.J. Daun, T.A. Sipkens, J.T. Titantah, M. Karttunen, Appl. Phys. B **112**, 409–420 (2013)
30. S. Maffi, F. Cignoli, C. Bellomunno, S. De Iuliis, G. Zizak, Spectrochim. Acta Part B **63**, 202–209 (2008)
31. F. Cignoli, C. Bellomunno, S. Maffi, G. Zizak, Appl. Phys. B **96**, 399–593 (2009)
32. J. Shi, J. Chen, Z. Feng, T. Chen, Y. Lian, X. Wang, C. Li, J. Phys. Chem. C **111**, 693–699 (2007)
33. A. Strini, L. Schiavi, R. Zanoni, S. De Iuliis, R. Dondè, S. Maffi, F. Migliorini, J. Appl. Biomater Funct. Mater. **15**(4), e408 (2017)
34. S. De Iuliis, M. Barbini, S. Benecchi, G. Zizak, Combust. Flame **115**, 253–261 (1998)
35. S. De Iuliis, S. Maffi, F. Cignoli, G. Zizak, Appl. Phys. B **102**, 891–903 (2011)

36. A. Saha, A. Moya, A. Kahnt, D. Iglesias, S. Marchesan, R. Vannemacher, M. Prato, J.J. Vilatela, D.M. Guldi, Nanoscale **9**, 7911–7921 (2017)
37. T.A. Sipkens, P.J. Hadwin, S.J. Grauer, K.J. Daun, Appl. Opt. **56**, 8436–8445 (2017)
38. S. Gordon, B.J. McBride, NASA Reference Publication 1311 (1996)